A Super-Earth and two Neptunes Orbiting the Nearby Sun-like star 61 Virginis

Steven S. Vogt[1], Robert A. Wittenmyer[3], R. Paul Butler[2], Simon O'Toole[5], Gregory W. Henry[7], Eugenio J. Rivera[1], Stefano Meschiari[1], Gregory Laughlin[1], C. G. Tinney[3], Hugh R. A. Jones[5], Jeremy Bailey[3], Brad D. Carter[6], Konstantin Batygin[8]

Received _____; accepted _____

draft: hd115617_rev13.tex

[1]UCO/Lick Observatory, University of California, Santa Cruz, CA 95064, USA

[2]Department of Terrestrial Magnetism, Carnegie Institution of Washington, 5241 Broad Branch Road, NW, Washington, DC 20015-1305, USA

[3]Department of Astrophysics, School of Physics, University of New South Wales, NSW 2052, Australia

[4]Anglo-Australian Observatory, P.O. Box 296, Epping, NSW 1710, Australia

[5]Centre for Astrophysical Research, University of Hertfordshire, Hateld, AL10 9AB, UK

[6]Faculty of Sciences, University of Southern Queensland, Toowoomba, Queensland 4350, Australia

[7]Center of Excellence in Information Systems, Tennessee State University, Nashville, TN 37209, USA

[8]Department of Geological and Planetary Sciences, Caltech, Pasadena, CA 91125, USA

ABSTRACT

We present precision radial velocity (RV) data that reveal a multiple exoplanet system orbiting the bright nearby G5V star 61 Virginis. Our 4.6 years of combined Keck/HIRES and Anglo-Australian Telescope precision RVs indicate the hitherto unknown presence of at least three planets orbiting this well-studied star. These planets are all on low-eccentricity orbits with periods of 4.2, 38.0, and 124.0 days, and projected masses ($M \sin i$) of 5.1, 18.2, and 24.0 $M_{\oplus}$, respectively. Test integrations of systems consistent with the RV data suggest that the configuration is dynamically stable. Depending on the effectiveness of tidal dissipation within the inner planet, the inner two planets may have evolved into an eccentricity fixed-point configuration in which the apsidal lines of all three planets corotate. This conjecture can be tested with additional observations. We present a 16-year time series of photometric observations of 61 Virginis, which comprise 1194 individual measurements, and indicate that it has excellent photometric stability. No significant photometric variations at the periods of the proposed planets have been detected. This new system is the first known example of a G-type Sun-like star hosting a Super-Earth mass planet. It joins HD 75732 (55 Cnc), HD 69830, GJ 581, HD 40307, and GJ 876 as a growing group of exoplanet systems that have multiple planets orbiting with periods less than an Earth-year. The ubiquity of such systems portends that space-based transit-search missions such as KEPLER and COROT will find many multi-transiting systems.

Subject headings: astrobiology – planetary systems – stars: individual (61 Vir)

1. Introduction

Over 400 extrasolar planets are now known. The majority have been discovered by using precision radial velocities (RVs) to detect the reflex barycentric motion of the host star. We have had a large sample of over 1000 nearby stars under precision RV survey for the past 13 years at Keck and for the past 11 years by the Anglo-Australian Planet Search (AAPS) at the Anglo-Australian Telescope (AAT). Of particular interest are the nearest brightest stars, as they allow one to achieve the highest precision on stars worthy of follow-up with space-based missions such as *Hubble Space Telescope (HST)*, *Spitzer*, and *James Webb Space Telescope (JWST)*. Of equal importance to stellar apparent brightness in RV precision is observing cadence. Keplerian signatures are mostly strictly periodic, and the signal-to-noise ratio (S/N) of the detection can be enhanced in the presence of a random noise background through increased cadence. However, obtaining adequate cadence on large telescopes like the Keck and the AAT is quite difficult, as observing time is limited for any group.

Our groups have been combining observations from both the Keck and AAT on select stars in the declination overlap region. One of the target stars is 61 Virginis (61 Vir), a very nearby G5V star, only 8.5 parsecs away. This star was put on the Keck program in 2004 December and added to the AAPS target list about four months later. Over the past five years, we have accumulated a total of 206 precision RVs that indicate a system of at least three planets orbiting this star. In this paper, we present all of these RV data and discuss the planetary system that they imply.

2. Basic properties of the host star 61 Vir

61 Vir (=HD 115617, HR 5019, HIP 64924) is a very bright (V=4.74) and very well-studied star. It has a spectral type of G5V and lies at a distance of only 8.52±0.05 pc (Perryman et al. 1997). This star has been characterized by a number of studies, with properties of interest to planetary system characterization listed by Valenti & Fischer (2005) and Sousa et al. (2008). Table 1 summarizes recent determinations of the fundamental stellar parameters for 61 Vir. Taken together, the properties of 61 Vir indicate that it is an old, inactive star ideally suited for precision RV planet searches. Using Ca H+K measurements taken between 1994 and 2006, Hall et al. (2007) found that 61 Vir is one of 13 targets for which the observed variability is zero within the uncertainties. In 29 observations over 7 seasons, they measure a mean $\log R'_{\rm HK}$ of −4.93. Henry et al. (1996) also measured activity in this star, and they found $\log R'_{\rm HK} = -4.96$, which is consistent with Hall et al. above. Similarly, Wittenmyer et al. (2006) derived a mean $\log R'_{\rm HK} = -5.03$ from five years ($N = 18$) of observations at McDonald Observatory. Our measurement of $\log R'_{\rm HK} = -4.95$ leads to an estimate (Wright 2005) of 1.5 $\rm m\,s^{-1}$ for the expected RV jitter due to stellar surface activity. Baliunas et al. (1996) measured a rotation period of $P = 29$ days for 61 Vir. The age of 61 Vir was estimated as $6.3^{+3.3}_{-3.1}$ Gyr by Valenti & Fischer (2005) and $8.96^{+2.76}_{-3.08}$ Gyr by Takeda et al. (2007). In summary, 61 Vir is a nearby, bright, solar-type star with physical properties quite similar to our own Sun.

3. Observations

The HIRES spectrometer (Vogt et al. 1994) of the Keck I telescope and the UCLES spectrometer (Diego et al. 1990) of the AAT have been used to monitor 61 Vir. A total of 126 AAT observations, dating from 2005 April 21 to 2009 August 14, representing a time span of 1576 days, have been obtained. The median internal velocity uncertainty for these

AAT data is $0.65\,\mathrm{m\,s^{-1}}$. A total of 80 Keck observations dating from 2004 December 29 to 2009 Aug 09, representing a data span of 1685 days, have also been obtained. The median internal velocity uncertainty for these Keck data is $0.54\,\mathrm{m\,s^{-1}}$.

Doppler shifts were measured (Butler et al. 1996) by placing an Iodine absorption cell just ahead of the spectrometer slit in the converging beam from the telescope. This gaseous Iodine absorption cell superimposes a rich forest of Iodine lines on the stellar spectrum, providing a wavelength calibration and proxy for the point spread function (PSF) of the spectrometer. The Iodine cell is sealed and temperature-controlled to 50 ± 0.1 °C (at Keck) and 60 ± 0.1 °C (at the AAT) so that the column density of Iodine remains constant. For the Keck planet search program, we operate the HIRES spectrometer at a spectral resolving power $R \approx 70,000$ and wavelength range of 3700-8000 Å, though only the region 5000-6200 Å (with Iodine lines) is used in the present Doppler analysis. For the AAT program, we typically achieve a spectral resolving power of $R \approx 50,000$. Doppler shifts from the spectra are determined with the spectral synthesis technique described by O'Toole et al. (2008). The Iodine region is divided into ∼700 chunks of 2 Å each. Each chunk produces an independent measure of the wavelength, PSF, and Doppler shift. The final measured velocity is the weighted mean of the velocities of the individual chunks.

Table 2 lists the complete set of 206 RVs for 61 Vir, corrected to the solar system barycenter. The table lists the JD of observation center, RV, and internal uncertainty. No offset has been applied between the AAT and Keck in this table. The internal uncertainty reflects only one term in the overall error budget and results from a host of systematic errors from characterizing and determining the PSF, detector imperfections, optical aberrations, effects of under-sampling the Iodine lines, etc. Two additional major sources of error are photon statistics and stellar jitter. The latter varies widely from star to star, and can be mitigated to some degree by selecting magnetically inactive older stars and by

time-averaging over the star's unresolved dominant asteroseismological p-mode oscillations. Since the single exposures required to reach a required S/N for bright stars like 61 Vir are much shorter than the characteristic time scale of low-degree surface p-modes, short exposures (ie., <5 minutes) will add an additional noise (or "jitter") component. This latter effect was recognized as a potential noise source by the AAPS some time ago, and so, since 2005 July, AAPS observations of bright targets like 61 Vir have been extended to the $10-15$ minutes periods required to average over these p-mode oscillations (O'Toole et al. 2008, 2009). For most of the past four years, only single exposures of $\sim$7 s at Keck were taken of 61 Vir at each epoch, though in 2008 July we began p-mode averaging by combining multiple shots of 61 Vir over a $5-10$ minutes dwell at each epoch. All observations are then further binned on two-hour timescales after being precision Doppler processed.

4. Photometry

In addition to our RV observations from Keck I and AAPS, we have acquired high-precision photometric observations of 61 Vir during 17 consecutive observing seasons from 1993 April to 2009 April with the T4 0.75 m automatic photometric telescope (APT) at Fairborn Observatory. Our APTs can detect short-term, low-amplitude brightness variability in solar-type stars due to rotational modulation of the visibility of surface magnetic activity (spots and plages), as well as longer term variations associated with the growth and decay of individual active regions and the occurence of stellar magnetic cycles (Henry 1999). The photometric observations help to establish whether observed RV variations are caused by stellar activity or planetary reflex motion (e.g., Henry et al. 2000a). Queloz et al. (2001) and Paulson et al. (2004) have presented several examples of periodic RV variations in solar-type stars caused by photospheric spots and plages. The photometric observations are also useful to search for transits of the planetary companions

(e.g., Henry et al. 2000b).

The T4 APT is equipped with a precision photometer based on an electromagnetic interference (EMI) 9924B bi-alkali photomultiplier tube that measures photon count rates successively through Strömgren b and y filters. The APT measures the difference in brightness between a program star and nearby constant comparison stars. Our automatic telescopes, photometers, observing procedures, and data reduction techniques are described in Henry (1999). Further details on the development and operation of the automated telescopes can be found in Henry (1995a,b) and Eaton et al. (2003).

For 61 Vir, we used the two comparison stars HD 113415 (C1, $V = 5.58$, $B - V = 0.56$, F7 V) and HD 114946 (C2, $V = 5.33$, $B - V = 0.87$, G8 III-IV). The individual Strömgren b and y differential magnitudes have been corrected for differential extinction with nightly extinction coefficients and transformed to the Strömgren system with yearly mean transformation coefficients. Since 61 Vir lies at a declination of $-18°$, the photometric observations from Fairborn were made at air mass 1.6 – 1.8. Therefore, to maximize the precision of the measurements, we combined the Strömgren b and y differential magnitudes into a single $(b + y)/2$ passband. We also computed the differential magnitudes of 61 Vir with respect to the mean brightness of the two comparison stars. Because we are interested only in variability timescales of days to weeks, we have normalized the final differential magnitudes so that the mean brightness of each observing season is equal to zero. This effectively removes any long-term brightness variability in the two comparison stars as well as in 61 Vir. (However, the standard deviation of the seasonal mean differential magnitudes was only 0.00033 mag before normalization.)

A total of 1194 normalized differential magnitudes from 17 observing seasons are plotted in the top panel of Figure 1. The data scatter about their mean with a standard deviation $\sigma = 0.00196$ mag, which provides an upper limit to possible brightness variation

in 61 Vir. A Lomb-Scargle periodogram of the photometric measurements is shown in the bottom panel of Figure 1 and reveals no significant periodicities within the data. We computed least-squares sine fits for the three RV planet candidates described below; the semi-amplitudes of the lightcurve fits were 0.00016 ± 0.00007, 0.00011 ± 0.00008, and 0.00014 ± 0.00007 mag for the three periods 4.215, 38.012, and 123.98 days, respectively. We conclude that the photometric constancy of 61 Vir supports planetary reflex motion as the cause of the RV variations described in the next section.

5. The Planetary System Orbiting 61 Vir

The combined RV data from the AAPS and Keck telescopes show a root-mean-square (rms) scatter of $4.1\,\mathrm{m\,s^{-1}}$ about the mean velocity. This includes an offset of 0.895 $\mathrm{m\,s^{-1}}$ between the two telescopes (Keck - AAT) that was left as a free parameter and emerged from the three-planet Keplerian fit. This rms significantly exceeds both the scatter due to the underlying precisions of both the Keck and AAPS Doppler measurement pipelines *and* the scatter expected in this star due to its predicted $1.5\,\mathrm{m\,s^{-1}}$ level of stellar jitter. Figure 2 shows the combined RV data set.

Figure 3 (top panel) shows the circular periodogram of the combined RV data set. This is the power at any period associated with fitting circular orbits to the data. Power at each sampled period is proportional to the relative improvement in the fit quality for a circular model versus a constant velocity model — that is, the relative drop in χ^2_ν. Figure 3 (bottom panel) shows the spectral window or power spectrum due to the sampling times (Deeming 1975). This spectral window illustrates spurious power that can appear in the data merely from the sampling times alone.

The periodogram of the RV data (top panel of Figure 3) shows a number of significant

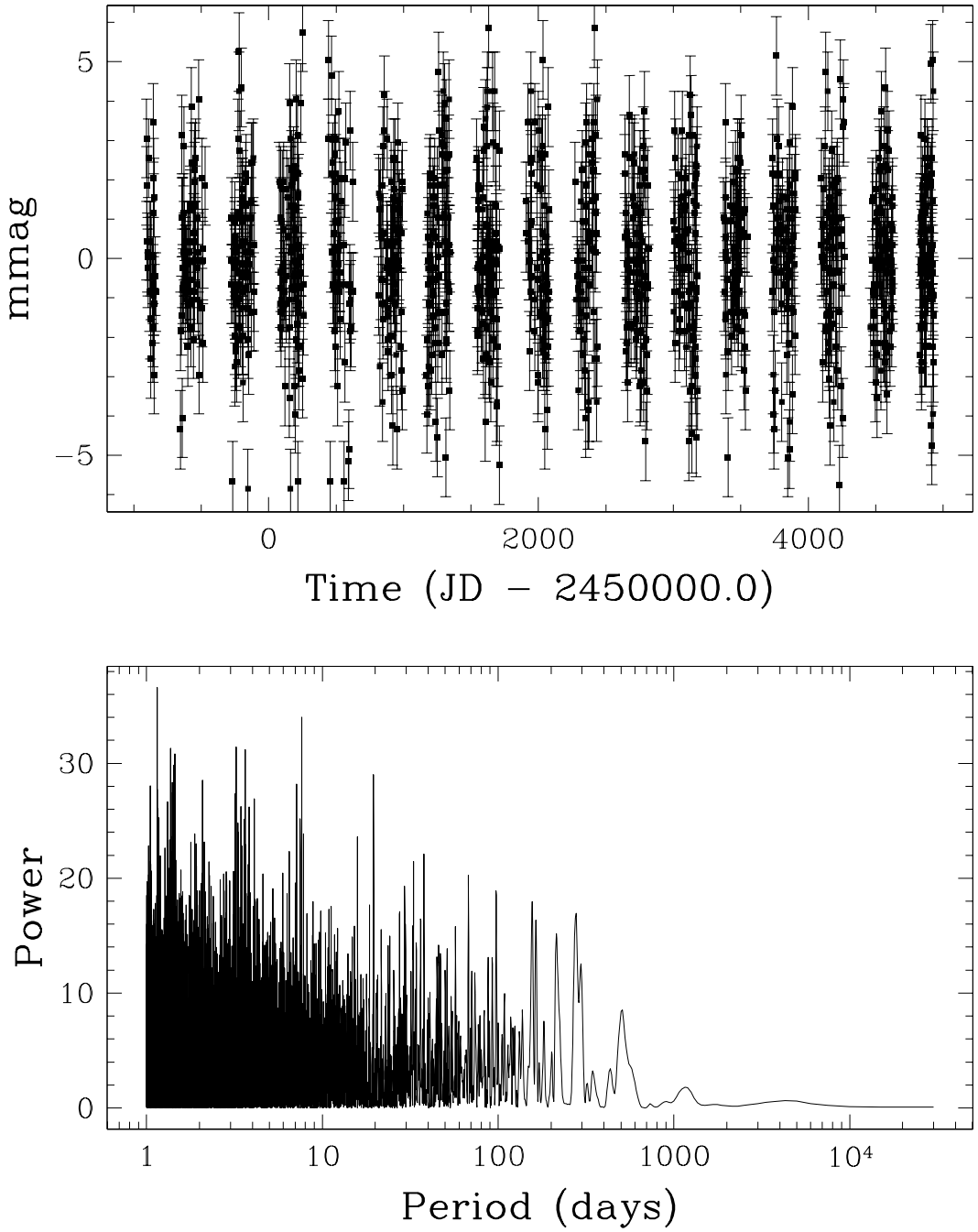

Fig. 1.— Differential photometry of 61 Vir (top panel). Periodogram of the photometry (bottom panel).

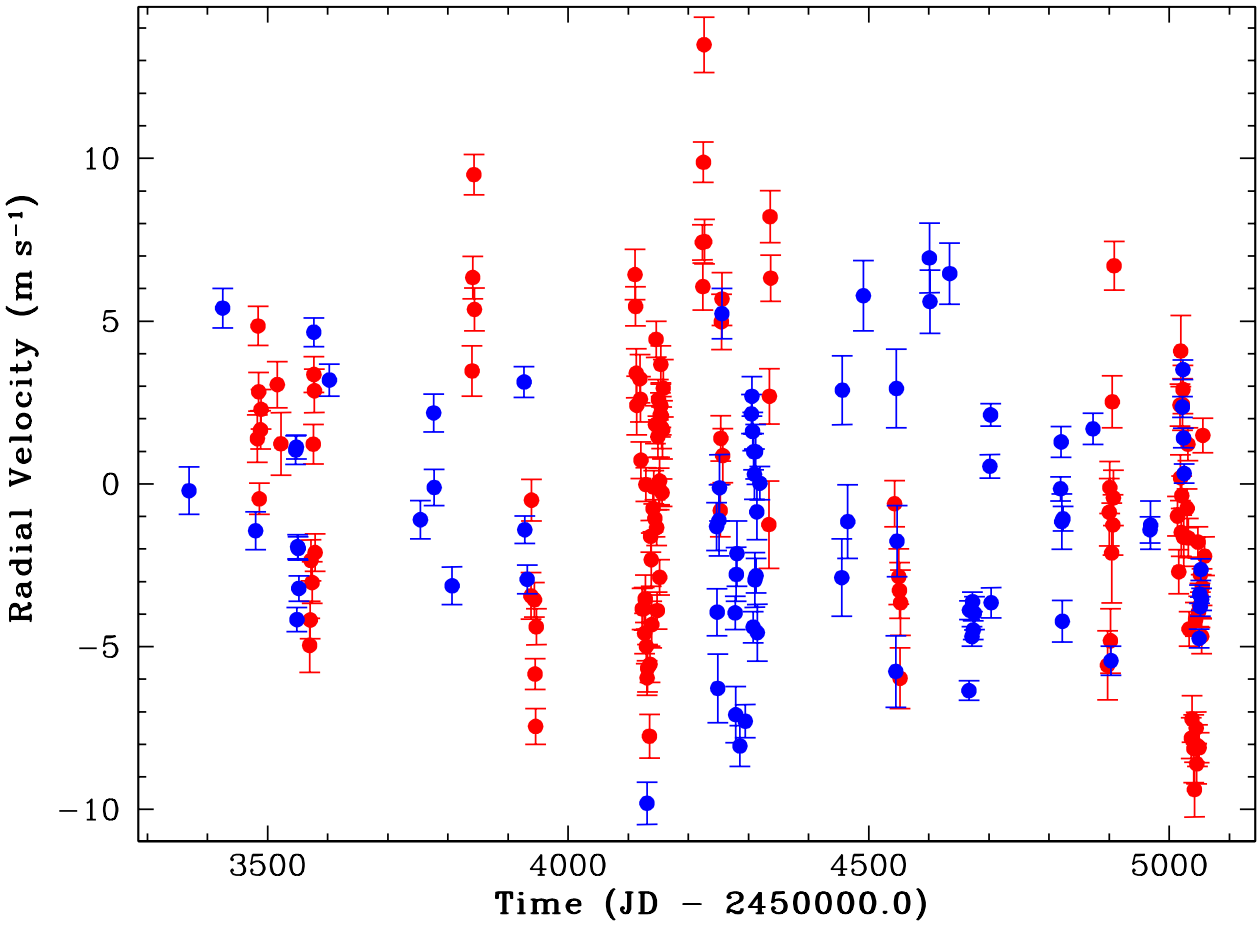

Fig. 2.— Relative radial velocities of 61 Vir. Velocities obtained at the AAT are shown in red, and those from Keck are shown in blue.

signals, with the strongest peak occurring at a period of $P = 38.13$ days. The false alarm probability (FAP) of this peak is estimated (adopting the procedure described in Cumming (2004)) to be FAP$\sim 3.8 \times 10^{-16}$. The horizontal lines in Figure 3 (top panel) and all similar figures below indicate (top to bottom) the 0.1%, 1%, and 10% FAP levels. This $P = 38.13$-day signal, furthermore, lies far from the periods favored by the sampling window (Figure 3; bottom panel), which produces spurious power at periods near 357, 191, 95.5, 652, 29.6, and 110 days. (Signals near these periods would naturally attract suspicion as being artifacts of the lunar and yearly periods on telescope scheduling.)

The mass of the host star is assumed to be 0.95 $M_\odot$, the isochrone mass of Valenti & Fischer (2005). Based on the periodogram, we then fit a planet of mass $M \sin i = 15 M_\oplus$ and $P = 38.20$ days on a circular orbit to the RV data. The presence of this planet (with RV semi-amplitude $K = 2.98$ m s^{-1}) reduces the rms scatter of the velocity residuals to 3.39 m s^{-1}. Figure 4 (top panel) shows the periodogram of the residuals to the one-planet fit which has strong peaks at $P = 124$ days and $P = 4.21$ days. The $P = 124$-day signal has FAP$\sim 6.3 \times 10^{-12}$ and can be modeled with a companion with $K = 3.36$ m s^{-1} and $M \sin i = 24 M_\oplus$. The addition of this planet further reduces the rms scatter to 2.78 m s^{-1}.

Figure 4 (bottom panel) shows the periodogram of the residuals to the two-planet fit which has a highly significant peak at a period of $P = 4.215$ days. As a consequence of the fact that the outer two planets, once removed, have significantly reduced the variance in the RV data, the FAP of the 4.215-day signal in the residuals is very small, FAP$\sim 1.1 \times 10^{-22}$. We are thus confident that this periodicity is real, and we ascribe it to the presence of a $P = 4.2149$ days, $M \sin i = 5.1 M_\oplus$ companion. There is another peak at 1.3 days that arises as an alias of the 4.2-day periodicity beating with the nightly sampling. The three-planet model has an rms scatter of 2.17 m s^{-1}.

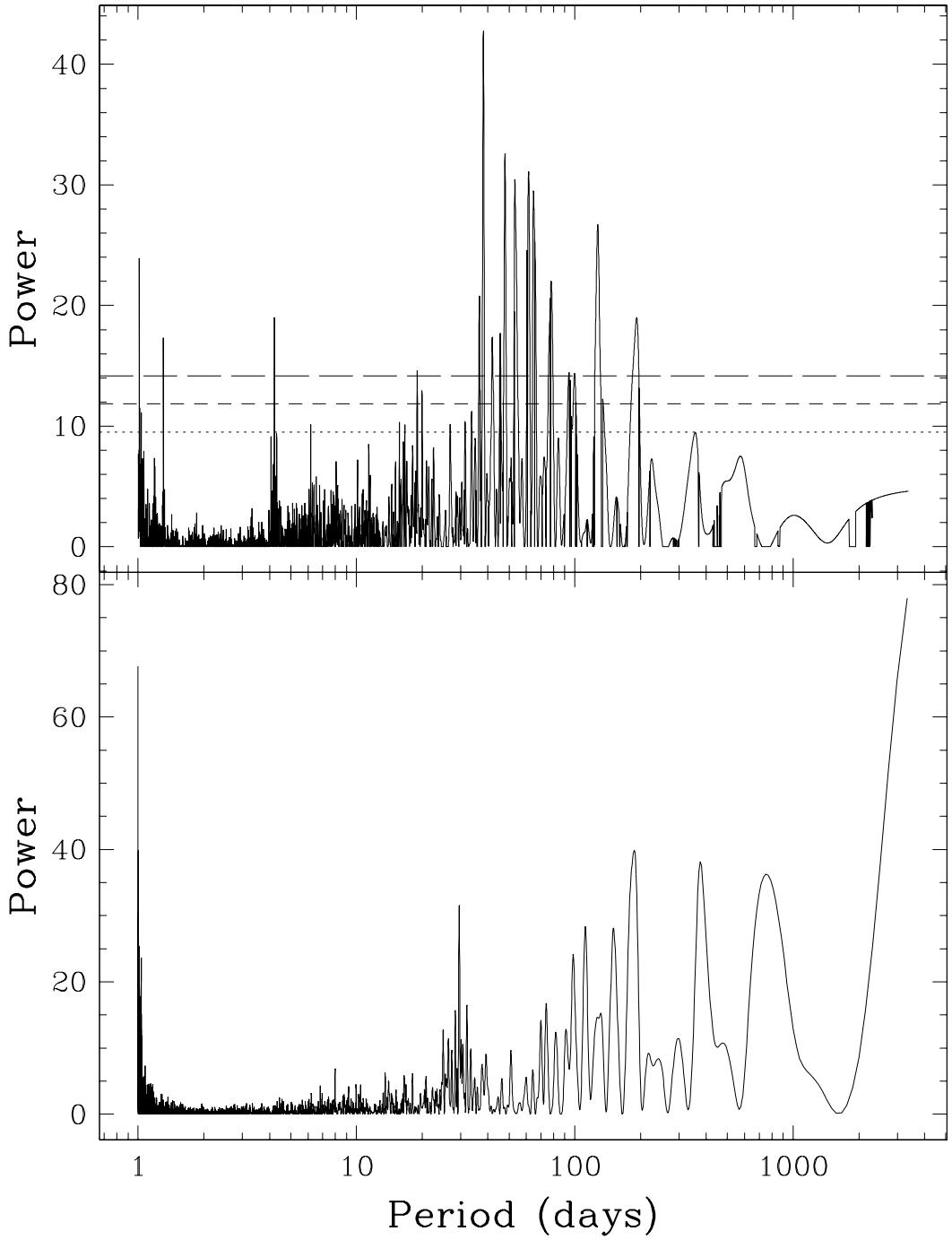

Fig. 3.— Top panel: circular periodogram of the combined RV data set for 61 Vir. Bottom panel: power spectral window of the combined RV data for 61 Vir.

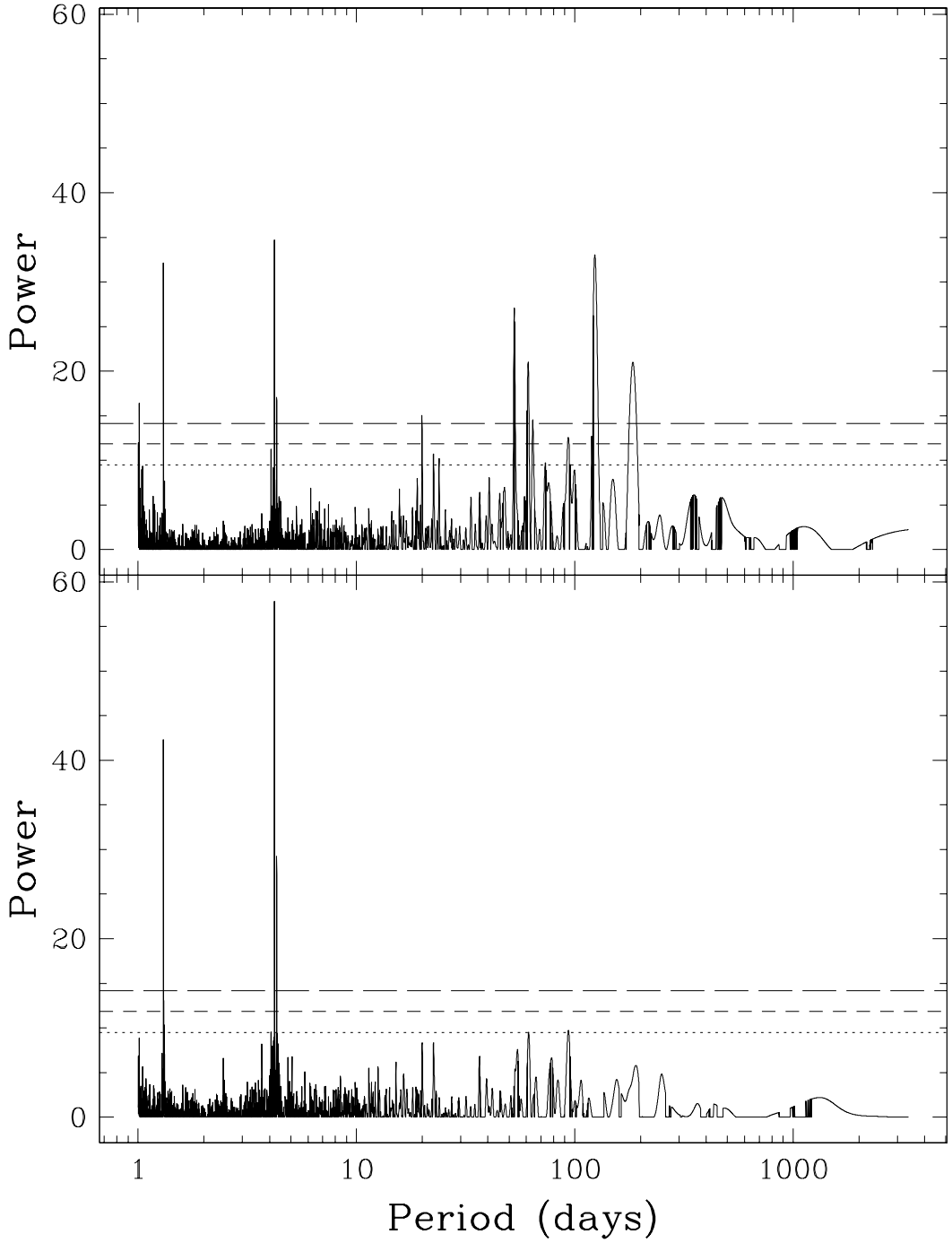

Fig. 4.— Top panel: circular periodogram of the one-planet residuals of the combined RV data set for 61 Vir. Bottom panel: circular periodogram of the two-planet residuals of the combined RV data set for 61 Vir.

Given the three-planet model, we can look either for solutions in which the planetary orbits are circular or solutions where the eccentricities are allowed to float. Inclusion of eccentricities provides only a modest improvement to the orbital fit, and we conclude that a significant amount of additional Doppler velocity monitoring will be required to improve measurement of the eccentricities. For a detailed discussion of how additional measurements can reduce uncertainties in orbital elements, see Ford (2005).

In Tables 3 and 4, we present our best-fit versions of the system under the assumption of circular orbits (Table 3) and with the additional degrees of freedom provided by fully Keplerian trajectories (Table 4). For the orbital fits, we assume $i = 90°$ and $\Omega = 0°$. We have verified that the inclusion of planet-planet gravitational interactions in the fit are unnecessary. Most of our modeling involves simply adding Keplerians. However, for cases where we expect significant gravitational interactions between companions, we carry out a more detailed modeling that involves using Hermite fourth order approximations to the planets' trajectories, accurately characterizing such gravitational interactions. If the Hermite fourth order calculations do not differ significantly from simple summed Keplerians, as is the case here, we conclude that planet-planet interactions are not necessary.

Uncertainties are based on 1000 bootstrap trials for which we follow the procedure in Section 15.6 from Press et al. (1992). We take the standard deviations of the fitted parameters to the bootstrapped RVs as the uncertainties. The fitted mean anomalies are reported at epoch JD 2453369.166. Our fitting was carried out with the publicly available *Systemic Console* (Meschiari et al. 2009).

Figure 5 (top panel) shows the power spectrum of the velocity residuals for the three-planet $e = 0$ fit. There is a significant peak near 94 days with FAP$\sim$ 0.0003. Although using this period in a four-planet circular fit results in a significant improvement in χ^2_ν, the rms decrease from 2.17 $\mathrm{m\,s^{-1}}$ for the three-planet model to 2.00 $\mathrm{m\,s^{-1}}$ is not significant.

Additionally, the fitted $K = 1.44$ m s^{-1} is significantly smaller than the scatter around the model. But perhaps most significantly, this fourth peak almost exactly corresponds to a peak in the window function of our data (Figure 3; lower panel), making any association of it with a real planet questionable.

The chi-squared of our three-planet circular fit is 13.03 and results in a fit with an rms of 2.17 m s^{-1} and estimated stellar jitter of 2.06 m s^{-1} . That estimate of the stellar jitter is the jitter required to bring the chi-squared of the fit down to 1.0. Thus, if the stellar jitter is 2.06 m s^{-1} , our three-planet fit is essentially perfect. The difference between a true stellar jitter of 2.06 m s^{-1} and our estimated value of 1.5 m s^{-1} is negligible, given the accuracy of such jitter estimates. Moreover, there are likely to be other planets in this system such as the 94-day signal in the top panel of Figure 5. Adding more planets to the model would further reduce the stellar jitter component of the fit. But the present data set does not support adding another Keplerian to the model.

Figure 5 (bottom panel) also shows the power spectrum of the velocity residuals for the eccentric three-planet fit. The tallest peak is near 10.9 days, but it is not significant with a FAP near 20%. Also, note that the rms for the eccentric three-planet fit of 2.09 m s^{-1} is not significantly different from the 2.17 m s^{-1} for the circular three-planet fit. At this point, all of these concerns indicate that many more observations are needed both to constrain the eccentricities of the first three planets and to pursue the prospect of a potential fourth planet in the system.

To summarize up to this point, we have shown that the combined Keck and AAT RV data show strong evidence for a three-planet system in orbit about the G5V star 61 Vir. Figure 6 shows the barycentric RV of the star computed with the eccentric three-planet model. Figure 7 shows the barycentric RV of the star computed with the eccentric model due to each individual companion in the system. In each panel, the velocities are folded

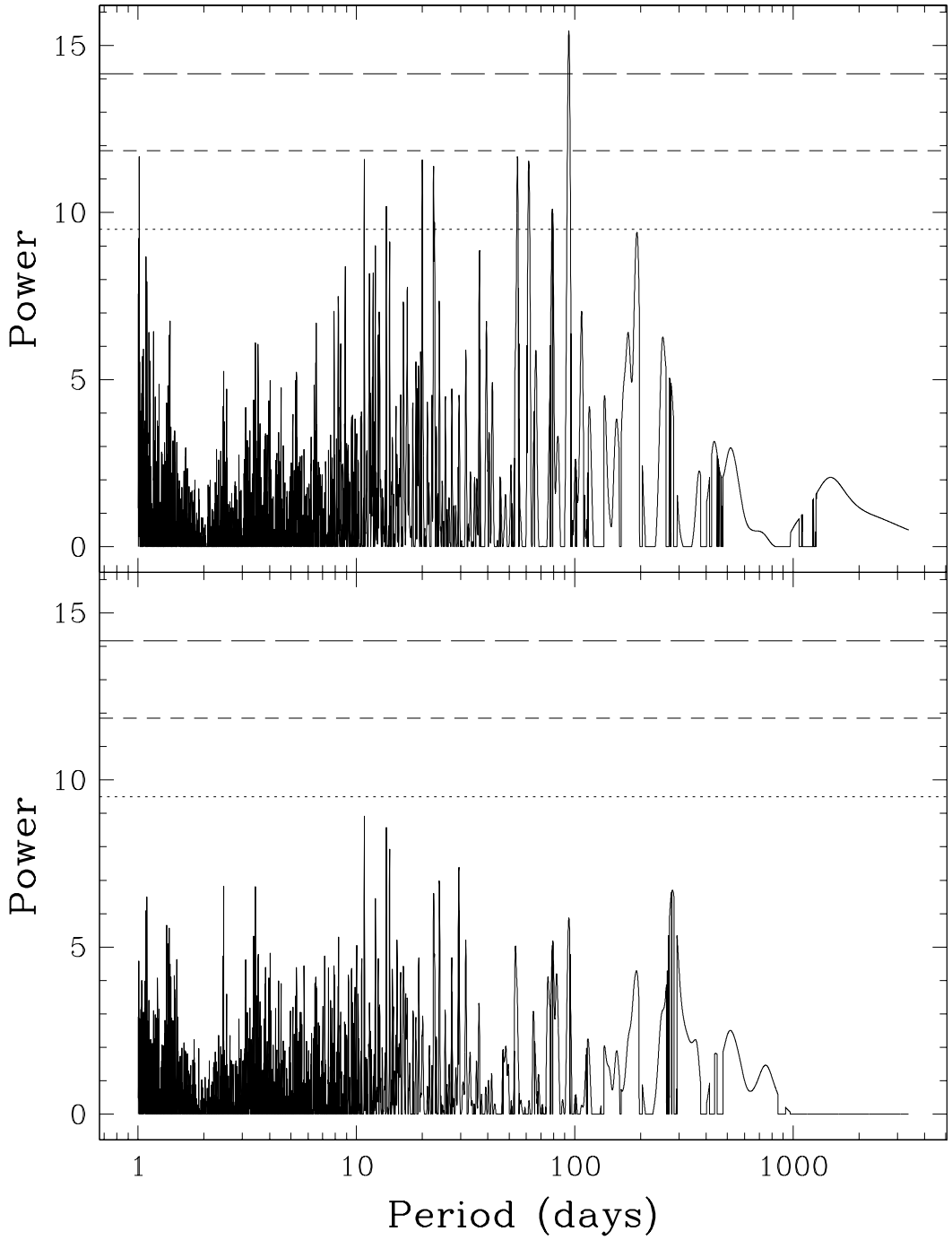

Fig. 5.— Top panel: circular periodogram of the three-planet residuals, assuming circular orbits, of the combined RV data set for 61 Vir. Bottom panel: circular periodogram of the three-planet residuals, with fitted eccentricities.

at the period of each corresponding planet. Points marked as open symbols denote observations that are suspect due to poor observing conditions that led to low S/N in the spectra. All such points were previously noted in the observing logs before any analysis occurred. Regardless of such suspicions, all observations were used in all the analyses.

6. Dynamical Analysis

For any multiple-planet system, long-term orbital stability is a matter of both interest and concern. Even precisely characterized, seemingly stable configurations such as the Solar System are subject to chaotic planet-planet interactions that can lead to orbit-crossing, collisions, and ejections on time scales shorter than the stellar lifetime (for recent treatments see, e.g., Laskar (2008); Batygin & Laughlin (2008); Laskar & Gastineau (2009)). Given the uncertainties that adhere to the orbital elements, the effort of generating a dynamical characterization of a system such as 61 Vir b-c-d, is somewhat akin to producing detailed maps of sand dunes. Nonetheless, it is useful to verify, via numerical integration, whether the planetary configurations listed in Tables 3 and 4 are dynamically stable. Such an analysis is particularly useful in giving rough bounds on the allowed coplanar inclinations relative to the line of sight to Earth. For simulations that do not include the effects of tidal dissipation, we use fitted Newtonian parameters for the initial states for long-term integrations. With a time step of 0.1 day, we use the MERCURY integration package (Chambers 1999) for the simulations. We include the first order post-Newtonian term in the star's potential as in Lissauer & Rivera (2001).

If we assume the three orbits are initially circular, with periods, masses, and mean anomalies given in Table 3, we find that the system is stable for at least 365 Myr. Additionally, assuming the system to be coplanar, if we set the inclination to the sky plane to various values from $i = 90°$ all the way down to $i = 1°$ and perform a Newtonian fit for

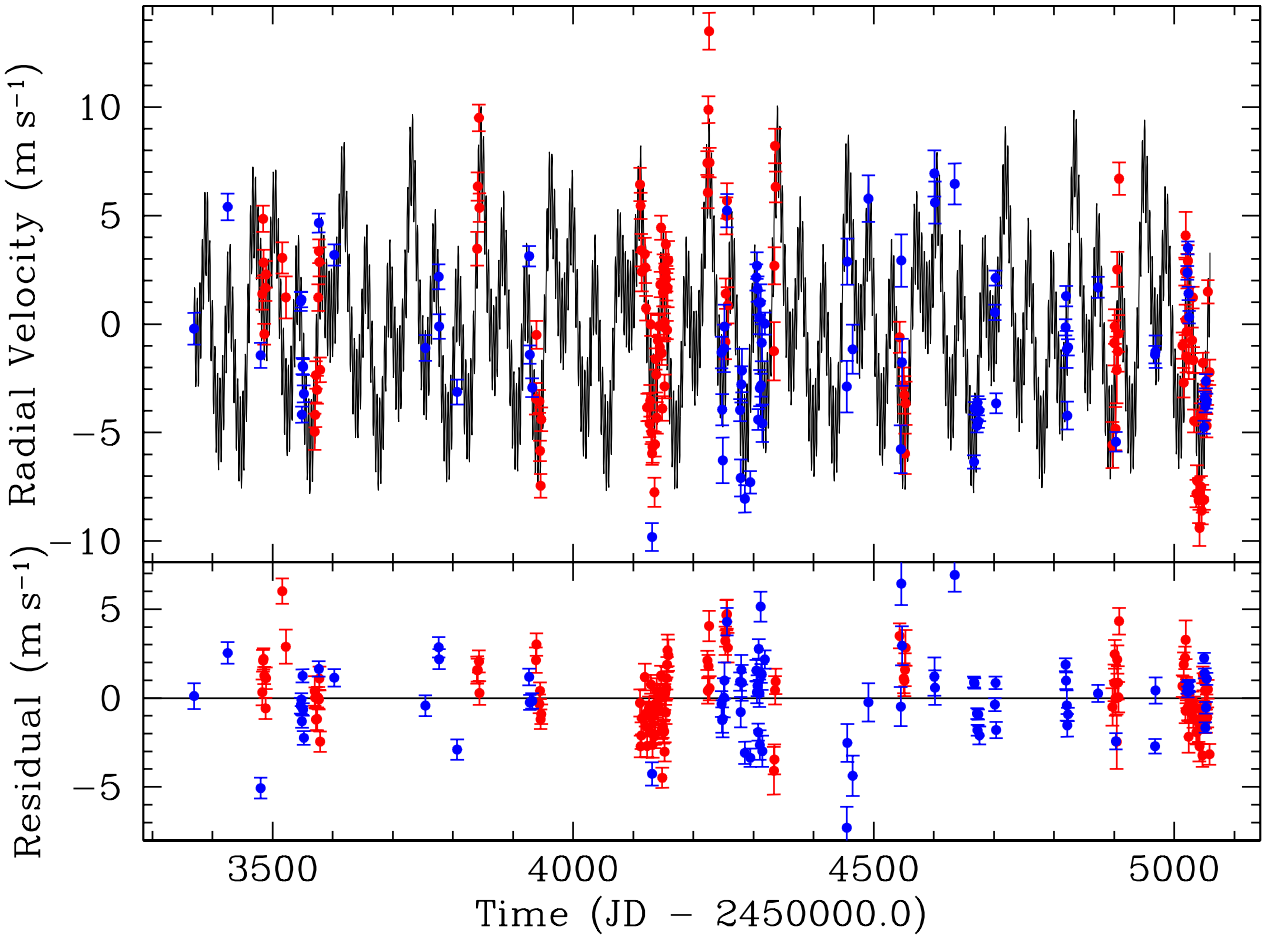

Fig. 6.— Top panel: observed RVs of 61 Vir (red points for AAT observations and blue for those from Keck) and model RV of 61 Vir due to the eccentric three-planet fit listed in Table 4 (black curve). The fitted relative offset of 0.895 m s^{-1} has been applied between the two data sets from the two telescopes. Bottom panel: residual velocities remaining after subtracting the eccentric three-planet model from the observations (again, red is for AAT, and blue is for Keck).

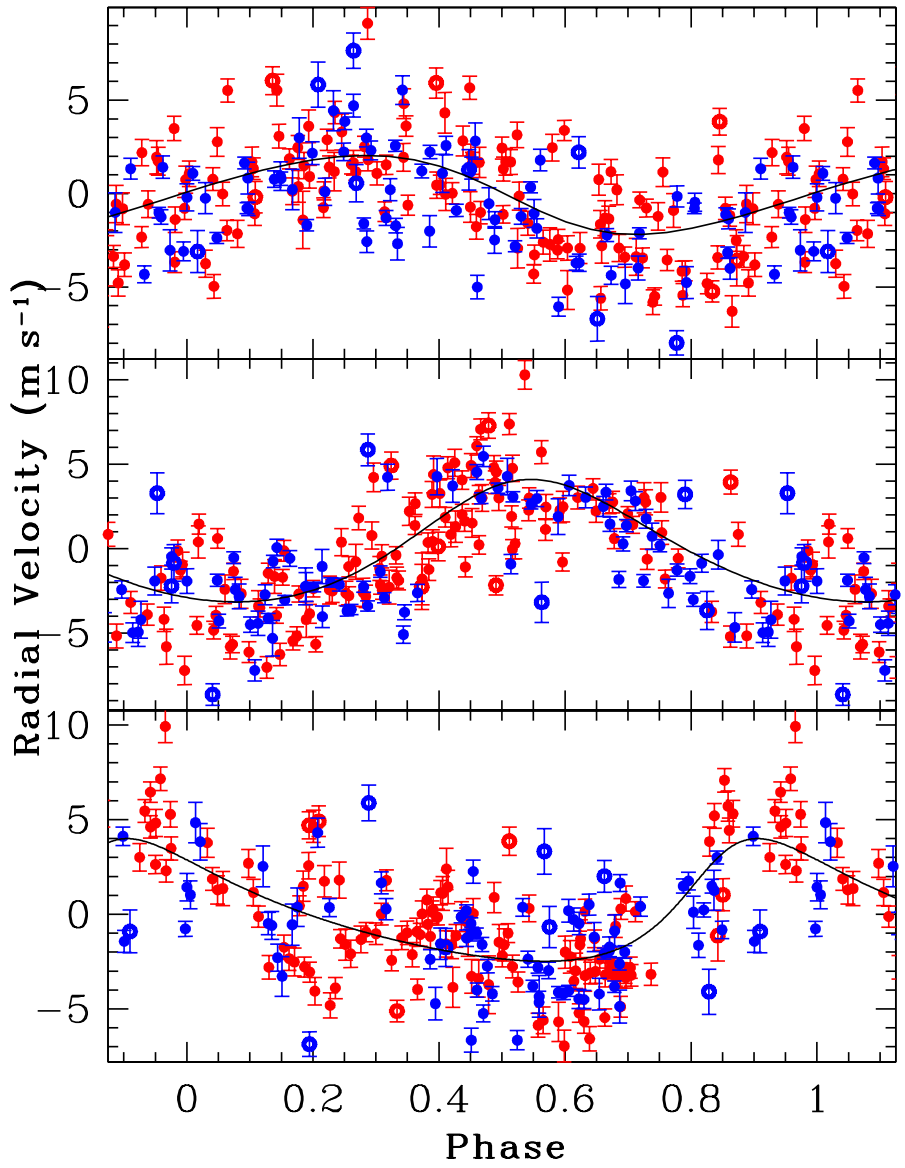

Fig. 7.— Top panel: radial velocity of 61 Vir due to planet b folded at 4.215 days. Center: radial velocity of 61 Vir due to planet c folded at 38.021 days. Bottom panel: radial velocity of 61 Vir due to planet d folded at 123.01 days. In each panel, the effect of the other two planets has been subtracted out. The curves represent the model velocities due to each respective planet. The AAT observations are shown in red, and the Keck velocities are shown in blue. Open symbols represent observations that may be suspect due to low S/N based on observing log notes.

the other 11 parameters (three parameters per planet plus the two velocity offsets), χ^2_ν does not change significantly from the nominal $i = 90°$ fit. We also find the $i = 1°$ fit to result in a system that is stable for at least 50 Myr. For this inclination, the fitted masses exceed 1.0, 3.3, and 4.5 $M_{\rm Jup}$. This system is stable because of the small eccentricities. Thus, under the assumption that the system is coplanar and the orbits are (nearly) circular, we cannot place a lower bound on the inclination of the system.

The parameters of the floating-eccentricity version of the 61 Vir system given in Table 4 were also used as the initial input conditions for a 10^7 yr simulation. The three-planet configuration remained stable for the full duration of this simulation. Figure 8 shows the evolution of the planets' semi-major axes and eccentricities over the first 250,000 years of the simulation. The planets interact with each other on secular timescales, and the inner planet experiences a large excursion in eccentricity (up to $e \sim 0.5$) but is never disrupted.

With its period of 4.215 days, the innermost planet in the system is likely subject to significant tidal dissipation in its interior. Tidal damping, in fact, may have played an important role in the evolutionary history of this multi-planet system. An investigation of this process requires a dynamical theory that couples dissipative orbital evolution with planet-planet gravitational perturbations among the individual system members. While the coupling between dissipative and secular processes can be complex, there exists an avenue toward insight regarding the overall dynamical state of the system. In particular, it may be possible that the dissipative properties of the innermost planet can be inferred.

The key idea is that, under the influence of tidal dissipation, multiple-planet systems approach stationary configurations. These so-called *tidal fixed points* are discussed in the context of extrasolar planets by Wu & Goldreich (2002) and more generally by Mardling (2007). Fixed-point configurations are characterized by either parallel or anti-parallel alignment of the apsides, and simultaneous precession of the apsidal lines. Additionally, the

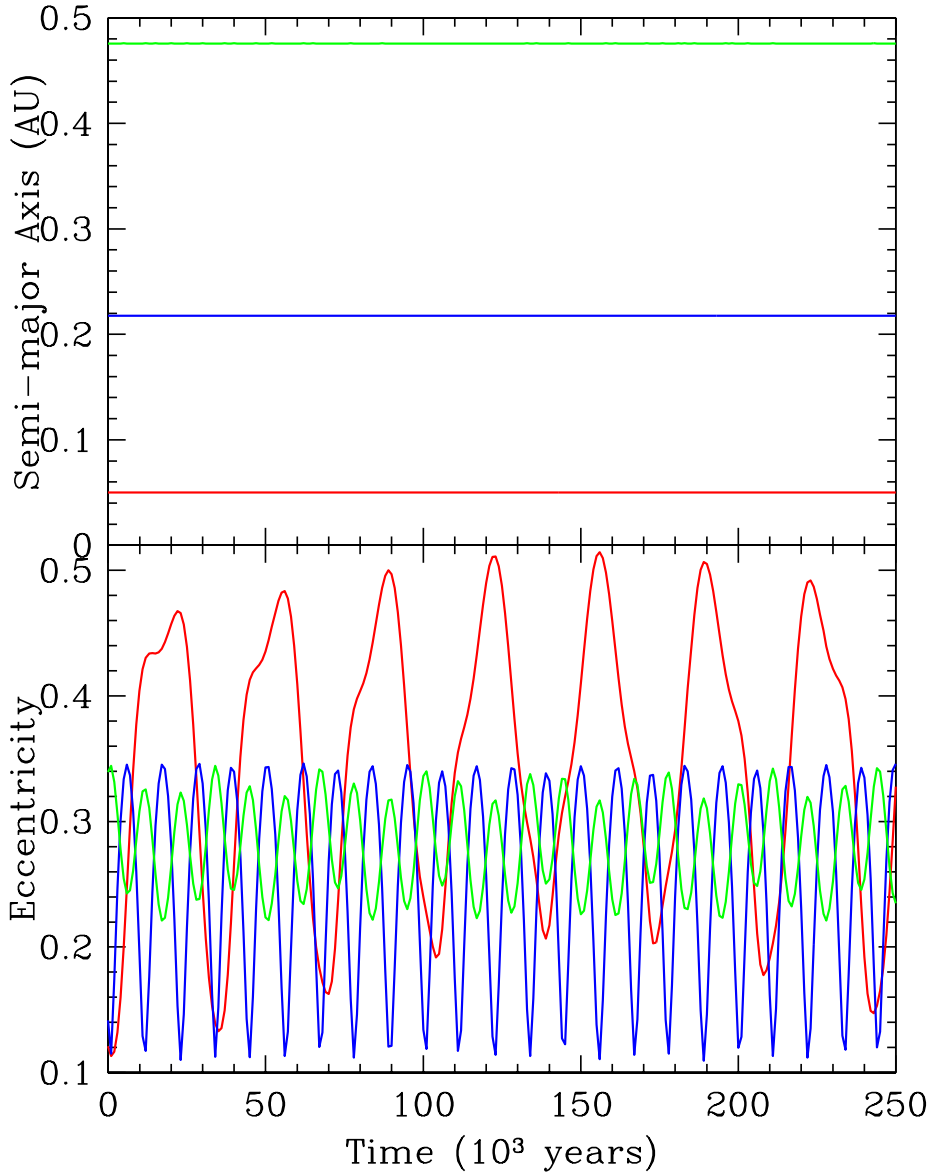

Fig. 8.— Top panel: semi-major axes vs. time for the simulation using the parameters from Table 4 as starting conditions. Bottom panel: eccentricities vs. time for the same simulation. For both panels, planet b is in red, c is in blue, and d is in green.

eccentricities of such systems are well determined and are not subject to significant time variations.

Participation by the system in a fixed-point configuration hinges on the tidal quality factor, Q, of planet b. Assuming that the system did not form in a stationary configuration, and that the dissipation of planetary orbital energy has been dominated during the past by tides raised on the innermost planet, it can be shown that it takes ~ 3 circularization timescales, τ, given by Yoder & Peale (1981),

$$\tau = \frac{2}{21n}\left(\frac{Q}{k}\right)\left(\frac{m}{M_\star}\right)\left(\frac{a}{R}\right)^5, \tag{1}$$

where k is the planetary Love number and R is the inner planet's radius, for the system to become stationary (Mardling 2007). Therefore, assuming $R = 2.45R_\oplus$ and $k = 0.34$, we expect that it would take $\sim 700,000 \times Q$ years for the system to arrive at the fixed point. We have confirmed this, by performing a numerical integration, using the tidal friction formalism of Eggleton et al. (1998) and Mardling & Lin (2002), and the eccentric fit listed in Table 4 as initial conditions. Indeed, libration of planet b around the fixed point begins after $\sim 850,000 \times Q$ years, in rough agreement with theory. It is further interesting to note that the best-fit eccentricities for planets c and d are in fact already very close to the fixed-point values, and their perihelia are already set in a librating mode at the beginning of the integration.

Thus, given the star's multi-billion year age, we can make the following claim: if planet b has a Neptune-like Q ($\sim 30,000$), then the system is probably not stationary. However, if the planet has a characteristic terrestrial Q (~ 100), then we can expect the system to be at a fixed point. If the system is at a fixed point, and the eccentricities are modest, we can use modified Laplace-Lagrange secular theory to relate the planets' eccentricities to each-other. The three-planet fixed point equations presented in Batygin et al. (2009), yield the relationships: $e_c \approx 5.11e_b$, and $e_d \approx 7.27e_b$. Thus, by a precise determination of

fixed-point eccentricities, we can not only determine the dynamical state of the system, but also begin to characterize the nature of planet b.

7. Discussion

We have detected three low-mass planets orbiting the nearby star 61 Vir. With a RV semi-amplitude $K = 2.09 \pm 0.23$ m s^{-1}, the $M \sin i = 5.10\, M_{\oplus}$ inner planet 61 Vir b is among the very lowest amplitude companions yet detected using the Doppler velocity technique. To date, the only announced planets with *smaller* amplitudes have been Gliese 581e, with $K = 1.85 \pm 0.23$ m s^{-1} (Mayor et al. 2009b), and HD 40307b, with $K = 1.97 \pm 0.11$ m s^{-1} (Mayor et al. 2009a). The inner planet in the HD 69830 system, with $K = 2.20 \pm 0.20$ m s^{-1} (Lovis et al. 2006) presents a slightly larger K. Interestingly, all four of the lowest amplitude planets known are members of multiple-planet systems containing three or more Neptune or super-Earth class objects on orbits that would be ascribed to the inner zone of the terrestrial region were they in our own solar system.

Given the observed multiplicity, negligible jitter, and extraordinary photometric stability associated with the 61 Vir planetary system, it is natural to speculate on the existence and detectability of additional planets. As 61 Vir is a naked-eye visible solar-type star observable from both hemispheres, it has been the target of many planet-search efforts in the past 25 years. One of the first precision RV searches for planets, by Walker et al. (1995), observed 61 Vir for approximately 12 years. They present a figure indicating rough upper limits of 1 – 2 Jupiter masses in the period range between one and ten years. Cumming et al. (1999) included 61 Vir in their determination of companion limits from 11 yr of the Lick planet search. They computed a 99% upper limit on the velocity amplitude $K = 19$ m s^{-1} and noted a possible candidate companion with a period of 9.8 yr and $K \sim 15$ m s^{-1}. Later, Wittenmyer et al. (2006) combined 23 years of velocities for 61 Vir,

including those data from Walker et al. (1995) and from the McDonald Observatory long-term planet search program, to derive companion-mass upper limits of $1.16\,M_{\rm Jup}$ at 3 AU and $1.69\,M_{\rm Jup}$ at 5.2 AU. From these studies, and the lack of any significant trends in the RV data, it would appear that there are no planets in the 61 Vir system with masses substantially greater than that of Jupiter. Undetected sub-Jovian mass planets may be present in orbits with periods longer than the extant high-precision velocity data.

A further interesting clue to the nature of the 61 Vir system was recently provided by Tanner et al. (2009), who detected an infrared excess at 160μ using *Spitzer* observations. The excess 160μ flux implies the presence of a dust disk that is continuously replenished by collisions within a cold Kuiper-Belt-like disk of planetesimals surrounding the star. Tanner et al. (2009) also suggest that the disk is resolved at 70μ (G. Bryden et al. 2009, in preparation). Assuming that the emitting grains are black bodies, the disk spans an annulus from $R_{\rm inner} = 96\pm5$ AU to $R_{\rm outer} = 195\pm10$ AU, with the dust temperature at 55-45 K (inner to outer). An improved model of the disk, however, can be achieved by assuming the emission arises from silicate grains with size 0.25μ. In this case, the disk spans $R_{\rm inner} = 120\pm20$ AU to $R_{\rm outer} = 220\pm10$ AU with a dust temperature of 24-19 K. An excess at 70μ was also detected with *Spitzer* by Trilling et al. (2008).

The 61 Vir system is consistent with the population of planets postulated by Mayor et al. (2009a), who inferred that fully one-third of solar-type stars in the immediate galactic neighborhood are accompanied by Neptune- (or lower) mass planets having orbital periods of 50 days or less. This putative population was largely unexpected, and has spurred a good deal of recent theoretical work geared to explain its existence. We note that the habitable zone of 61 Vir is located in the vicinity of a 300-day orbit. At this separation from the parent star, a $2\,M_\oplus$ planet induces a RV semi-amplitude $K = 0.2\ {\rm m\,s^{-1}}$. Assuming a combined stellar jitter and median internal uncertainty of $1.5\ {\rm m\,s^{-1}}$, this is a factor of

about 30 greater than the 0.05 $\mathrm{m\,s^{-1}}$ precision required to make a 4σ measurement of a such a small signal. If precision scales as the square root of the total number of Doppler measurements, a total of 30^2 or 900 velocities (an additional 700 more) would allow for the detection of such a planet with a S/N of 4.

With a period of only 4.215 days ($a = 0.05$ AU), 61 Vir b may transit its star. The *a priori* transit probability is $\sim 9\%$ (assuming $R_\star = 1\,R_\odot$). Due to the low mass of 61 Vir b, a successful transit observation would allow a detailed physical probe of a fundamentally new class of planet. Currently, the lowest mass transiting planet is CoRoT-7b, with a radius of $1.68 \pm 0.09\,R_\oplus$ (Leger et al. 2009). CoRoT-7b orbits a G9V star and has a transit depth of only $\Delta F/F = 3.4 \times 10^{-4}$. Its mass is estimated by Queloz et al. (2009) to be $4.8 \pm 0.8 M_\oplus$. By comparison, if 61 Vir b is transiting, $\sin i \sim 1$, and hence it would have a mass of $5.10\,M_\oplus$. Assuming that the planet migrated inward from beyond the ice line of 61 Vir's protoplanetary disk, it is likely made mostly of water. The models of Fortney et al. (2007) indicate a $2.45\,R_\oplus$ radius for such a planet, leading to a central transit depth of ~ 0.54 millimagnitudes. Such a transit could be detected from space using, for example, the Warm Spitzer platform.

Of the currently known planets discovered by the RV technique with $M \sin i < 10 M_\oplus$ (10 planets; 6 host stars), half orbit M dwarf stars. Those are GJ 581c,d,e (Mayor et al. 2009b), GJ 876d (Rivera et al. 2005), and GJ 176b (Forveille et al. 2009). The rest of those planets orbit K stars: HD 7924b (Howard et al. 2009), HD 181433b (Bouchy et al. 2009), and HD 40307b,c,d (Mayor et al. 2009a). This is of course a selection effect, since late-type stars have lower masses and hence a planet of a given mass would produce a larger RV signal. 61 Vir, therefore, is a unique new system in that not only does it host multiple low-mass planets, but also it is the first G-type Sun-like star found through the RV technique to host a planet with $M \sin i < 10 M_\oplus$.

The detection of the three low-K planets reported here around this previously well-studied, bright, nearby star was made possible by the combined cadence and high precision of the AAPS and Keck surveys. As cadence and time bases grow in the RV monitoring of chromospherically quiet, nearby stars, complex planetary systems, like 55 Cnc, and now 61 Vir, are becoming increasingly common. This is only our first reconnaissance of this fascinating and quite nearby system. As more RV data are collected, the orbital ephemerides of the planets will become better determined, and more planets will probably be revealed.

The 61 Vir system joins a growing class of exoplanet systems that have multiple planets orbiting with periods less than an Earth-year. Other examples are HD 75732 (55 Cnc), HD 69830, GJ 581, HD 40307, and GJ 876. The increasing frequency of such systems portends that space-based transit surveys such as COROT and KEPLER will find many multi-transiting systems.

We gratefully acknowledge the major contributions of fellow members of our previous California-Carnegie Exoplanet team: Geoff Marcy, Jason Wright, Debra Fischer, and Katie Peek in helping to obtain the RVs presented in this paper. S.S.V. gratefully acknowledges support from NSF grant AST-0307493. R.P.B. gratefully acknowledges support from NASA OSS Grant NNX07AR40G, the NASA Keck PI program, and the Carnegie Institution of Washington. G.L. acknowledges support from NSF AST-0449986. G.W.H. acknowledges support from NASA, NSF, Tennessee State University, and the state of Tennessee through its Centers of Excellence program. The work herein is based on observations obtained at the W. M. Keck Observatory, which is operated jointly by the University of California and the California Institute of Technology, and we thank the UC-Keck and NASA-Keck Time Assignment Committees for their support. We gratefully acknowledge the UK and Australian government support of the AAT through their PPARC, STFC,

DETYA, and DIISR funding. C.G.T. and H.R.A.J. acknowledge support from STFC grant PP/C000552/1, while C.G.T. acknowledges support from ARC Grant DP0774000. Travel support to the AAT has been generously provided by the Anglo-Australian Observatory (to C.G.T., B.D.C., and J.B.). We are grateful for the extraordinary support we have received from the AAT technical staff at the AAT — E. Penny, R. Paterson, D. Stafford, F. Freeman, S. Lee, J. Pogson, S. James, J. Stevenson, K. Fiegert, and W. Campbell. We also wish to extend our special thanks to those of Hawaiian ancestry on whose sacred mountain of Mauna Kea we are privileged to be guests. Without their generous hospitality, the Keck observations presented herein would not have been possible. This research has made use of the SIMBAD database, operated at CDS, Strasbourg, France.

Facilities: AAT (UCLES), Keck (HIRES).

REFERENCES

Baliunas, S., Sokoloff, D., & Soon W. 1996, ApJ, 457, L99

Batygin, K. & Laughlin, G. 2008, ApJ, 683, 1207

Batygin, K., Laughlin, G., Meschiari, S., Rivera, E., Vogt, S., & Butler, P. 2009, ApJ, 699, 23

Bouchy, F., et al. 2009, A&A, 496, 527

Butler, R. P., Marcy, G. W., Williams, E., McCarthy, C., Dosanjh, P., & Vogt, S. S. 1996, PASP, 108, 500

Cenarro, A. J., et al. 2007, MNRAS, 374, 664

Chambers, J. E. 1999, MNRAS, 304, 793

Cumming, A. 2004, MNRAS, 354, 1165

Cumming, A., Marcy, G. W., & Butler, R. P. 1999, ApJ, 526, 890

Deeming, T. J. 1975, Ap&SS, 36, 137

Desidera, S., Gratton, R. G., Lucatello, S., Claudi, R. U., & Dall, T. H. 2006, A&A, 454, 553

Diego, F., Charalambous, A., Fish, A. C., & Walker, D. D. 1990 Proc. SPIE, 1235, 562

Eaton, J. A., Henry, G. W., & Fekel, F. C. 2003, in The Future of Small Telescopes in the New Millennium, Volume II — The Telescopes We Use, ed. T. D. Oswalt (Dordrecht: Kluwer), 189

Ecuvillon, A., Israelian, G., Santos, N. C., Shchukina, N. G., Mayor, M., & Rebolo, R. 2006, A&A, 445, 633

Eggleton, P. P., Kiseleva, L. G., & Hut, P. 1998, ApJ, 499, 853

Ford, E. B. 2005, AJ, 129, 1706

Fortney, J. J., Marley, M. S., & Barnes, J. W. 2007, ApJ, 659, 1661

Forveille, T., et al. 2009, A&A, 493, 645

Hall, J. C., Lockwood, G. W., & Skiff, B. A. 2007, AJ, 133, 862

Henry, G. W. 1995a, in ASP Conf. Ser. 79, Robotic Telescopes: Current Capabilities, Present Developments, and Future Prospects for Automated Astronomy, ed. G. W. Henry & J. A. Eaton (San Francisco: ASP), 37

Henry, G. W. 1995b, in ASP Conf. Ser. 79, Robotic Telescopes: Current Capabilities, Present Developments, and Future Prospects for Automated Astronomy, ed. G. W. Henry & J. A. Eaton (San Francisco: ASP), 44

Henry, G. W. 1999, PASP, 111, 845

Henry, G. W., Baliunas, S. L., Donahue, R. A., Fekel, F. C., & Soon, W. 2000a, ApJ, 531, 415

Henry, G. W., Marcy, G. W., Butler, R. P., & Vogt, S. S. 2000b, ApJ, 529, L41

Henry, T. J., Soderblom, D. R., Donahue, R. A., & Baliunas, S. L. 1996, AJ, 111, 439

Howard, A. W., et al. 2009, ApJ, 696, 75

Laskar, J. 2008, Icarus, 196, 1

Laskar, J. & Gastineau, M. 2009, Nature, 459, 817

Leger, A., et al. 2009, A&A, 506, 287

Lissauer, J. J. & Rivera, E. J. 2001, ApJ, 554, 1141

Lovis et al. 2006, Nature, 441, 305

Mardling, R. A. 2007, MNRAS, 382, 1768

Mardling, R. A. & Lin, D. N. C. 2002, ApJ, 573, 829

Mayor, M., et al. 2009a, A&A, 493, 639

Mayor, M., et al. 2009b, A&A, 507, 487

Meschiari, S., Wolf, A. S., Rivera, E. J., Laughlin, G., Vogt, S. S., & Butler, R. P. 2009, PASP, 121, 1016

O'Toole, S. J., Tinney, C. G., & Jones, H. R. A. 2008, MNRAS, 386, 516

O'Toole, S., et al. 2009, ApJ, 697, 1263

Paulson, D. B., Saar, S. H., Cochran, W. D., & Henry, G. W. 2004, AJ, 127, 1644

Perryman, M. A. C. et al. 1997, A&A, 323, 49

Press, W. H., Teukolsky, S. A., Vetterling, W. T., & Flannery, B. P. 1992, Numerical Recipes: The Art of Scientific Computing (2nd Edition; Cambridge, U.K.: Cambridge University Press)

Queloz, D., et al. 2001, A&A, 379, 279

Queloz, D., et al. 2009, A&A, 506, 303

Rivera, E. J. et al. 2005, ApJ, 634, 625

Sousa, S. G., et al. 2008, A&A, 487, 373

Takeda, G., Ford, E. B., Sills, A., Rasio, F. A., Fischer, D. A., & Valenti, J. A. 2007, ApJS, 168, 297

Tanner, A., Beichman, C., Bryden, G., Lisse, C., & Lawler, S. 2009, ApJ, 704, 109

Trilling, D. E., et al. 2008, ApJ, 674, 1086

Valenti, J. A. & Fischer, D. A. 2005, ApJS, 159, 141

Vogt, S. S. et al. 1994, Proc. SPIE, 2198, 362

Walker, G. A. H., Walker, A. R., Irwin, A. W., Larson, A. M., Yang, S. L. S., & Richardson, D. C. 1995, Icarus, 116, 359

Wittenmyer, R. A., Endl, M., Cochran, W. D., Hatzes, A. P., Walker, G. A. H., Yang, S. L. S., & Paulson, D. B. 2006, AJ, 132, 177

Wright, J. T. 2005, PASP, 117, 675

Wu, Y. & Goldreich, P. 2002, ApJ, 564, 1024

Yoder, C. F. & Peale, S. J. 1981, Icarus, 47, 1

Table 1. Stellar Parameters for 61 Vir

Parameter	Value	Reference
Spec. Type	G5V	Cenarro et al. (2007)
Mass ($M_\odot$)	$0.95^{+0.04}_{-0.03}$	Valenti & Fischer (2005)
	$0.942^{+0.034}_{-0.029}$	Takeda et al. (2007)
Radius ($R_\odot$)	0.963±0.011	Valenti & Fischer (2005)
	0.98±0.03	Takeda et al. (2007)
Luminosity ($L_\odot$)	0.805±0.028	Valenti & Fischer (2005)
	0.804±0.005	Sousa et al. (2008)
Distance (pc)	8.52±0.05	Perryman et al. (1997)
$V \sin i$ (km s^{-1})	2.2	Valenti & Fischer (2005)
	1.9	Desidera et al. (2006)
$\log R'_{\rm HK}$	-4.93	Hall et al. (2007)
	-4.96	Henry et al. (1996)
	-5.03	Wittenmyer et al. (2006)
	-4.95	This work
$P_{\rm rot}$ (days)	29	Baliunas et al. (1996)
Age (Gyr)	$6.3^{+3.3}_{-3.1}$	Valenti & Fischer (2005)
	$8.96^{+2.76}_{-3.08}$	Takeda et al. (2007)
[Fe/H]	0.05	Valenti & Fischer (2005)
	-0.01	Cenarro et al. (2007)
$T_{\rm eff}$ (K)	5571	Valenti & Fischer (2005)
	5531	Cenarro et al. (2007)
	5577±33	Ecuvillon et al. (2006)
$\log g$	4.47	Valenti & Fischer (2005)
	4.31	Cenarro et al. (2007)
	$4.45^{+0.04}_{-0.03}$	Takeda et al. (2007)
	4.34±0.03	Ecuvillon et al. (2006)

Table 2. Radial Velocities for 61 Vir

JD (-2450000)	RV ($m\,s^{-1}$)	Error ($m\,s^{-1}$)	Observatory
3482.96440	2.10	0.73	A
3483.96117	5.56	0.60	A
3485.07996	3.54	0.59	A
3486.04514	0.25	0.48	A
3488.13906	2.37	0.59	A
3489.08696	3.00	0.61	A
3516.04043	3.76	0.71	A
3521.94298	1.94	0.96	A
3569.90141	-4.25	0.83	A
3570.94617	-3.47	0.57	A
3571.94048	-1.64	0.63	A
3573.87030	-2.32	0.64	A
3575.87530	1.93	0.61	A
3576.89023	4.07	0.55	A
3577.86776	3.57	0.67	A
3578.91377	-1.40	0.57	A
3840.21603	4.18	0.77	A
3841.16188	7.05	0.65	A
3843.13891	10.21	0.62	A
3844.08319	6.07	0.66	A

Table 2—Continued

JD (-2450000)	RV ($m\,s^{-1}$)	Error ($m\,s^{-1}$)	Observatory
3937.93317	-2.73	0.72	A
3938.93436	0.21	0.64	A
3943.88525	-2.85	0.53	A
3944.88569	-5.13	0.47	A
3945.88638	-6.74	0.55	A
3946.88960	-3.68	0.55	A
4111.21051	7.14	0.77	A
4112.21939	6.16	0.60	A
4113.22990	4.11	0.75	A
4114.26145	3.12	0.90	A
4119.24597	3.94	0.74	A
4120.22002	3.31	0.70	A
4121.21210	1.44	0.56	A
4123.23541	-3.13	0.63	A
4126.19788	-3.12	0.65	A
4127.20219	-3.88	0.62	A
4128.20519	-2.82	0.73	A
4129.20022	0.69	0.52	A
4130.19130	-4.28	0.53	A
4131.20082	-5.25	0.53	A

Table 2—Continued

JD (-2450000)	RV ($m\,s^{-1}$)	Error ($m\,s^{-1}$)	Observatory
4132.20696	-4.95	0.73	A
4135.19894	-7.04	0.67	A
4136.21567	-4.83	0.56	A
4137.21358	-0.90	0.49	A
4138.19311	-1.62	0.82	A
4139.18689	-3.61	0.72	A
4141.21764	-0.05	0.71	A
4142.20644	0.61	0.51	A
4144.14374	-0.35	0.57	A
4145.17237	2.53	0.58	A
4146.19289	5.15	0.55	A
4147.21096	-0.63	0.55	A
4148.24103	-3.18	0.57	A
4149.18109	2.16	0.63	A
4150.21285	3.30	0.62	A
4151.22296	0.56	0.64	A
4152.09352	0.80	0.73	A
4152.25396	-2.16	0.54	A
4153.17187	2.83	0.68	A
4154.09474	4.38	0.57	A

Table 2—Continued

JD (-2450000)	RV ($m\,s^{-1}$)	Error ($m\,s^{-1}$)	Observatory
4154.27050	3.11	0.66	A
4155.06551	2.80	0.59	A
4155.27322	2.43	0.64	A
4156.18613	0.44	0.42	A
4157.16889	2.37	0.89	A
4158.18706	3.65	0.88	A
4223.12188	8.13	0.54	A
4224.15218	6.77	0.72	A
4225.08458	10.59	0.62	A
4226.02062	14.20	0.85	A
4227.02043	8.15	0.68	A
4252.97759	-0.11	0.80	A
4254.01661	2.11	0.70	A
4254.91868	5.69	0.85	A
4255.98460	6.39	0.81	A
4257.07180	1.58	0.83	A
4333.86604	-0.54	1.34	A
4334.86018	3.40	0.85	A
4335.85304	8.92	0.80	A
4336.84663	7.03	0.71	A

Table 2—Continued

JD (-2450000)	RV ($m\,s^{-1}$)	Error ($m\,s^{-1}$)	Observatory
4543.06967	0.10	0.71	A
4550.11293	-2.14	0.85	A
4551.09816	-2.56	0.86	A
4552.14240	-5.26	0.93	A
4553.10980	-2.94	1.00	A
4897.20941	-4.86	1.06	A
4900.19861	-0.16	1.03	A
4901.16839	0.60	0.80	A
4902.21654	-4.11	0.99	A
4904.20346	-1.41	1.53	A
4905.27335	3.23	0.80	A
4906.22330	-0.55	0.93	A
4907.21266	0.28	0.85	A
4908.21531	7.41	0.75	A
5013.83842	-0.28	0.61	A
5015.83950	-1.99	0.68	A
5017.84841	3.13	0.64	A
5018.90225	0.90	0.70	A
5018.95764	4.79	1.09	A
5019.99765	-0.78	0.73	A

Table 2—Continued

JD (-2450000)	RV ($m\,s^{-1}$)	Error ($m\,s^{-1}$)	Observatory
5020.83414	0.35	0.60	A
5021.88251	3.15	0.79	A
5022.89587	3.61	0.74	A
5023.87589	-0.93	0.89	A
5029.86175	-0.04	0.59	A
5030.97802	1.93	0.50	A
5031.84137	-0.95	0.60	A
5032.92564	-3.75	0.53	A
5036.86026	-7.10	0.63	A
5037.84849	-6.51	0.71	A
5040.85306	-7.42	1.04	A
5041.95419	-8.68	0.84	A
5043.84520	-3.45	0.52	A
5044.84224	-6.79	0.49	A
5045.83918	-7.89	0.62	A
5046.91766	-7.33	0.64	A
5047.86724	-1.08	0.47	A
5048.85263	-3.21	0.47	A
5049.86609	-7.39	0.46	A
5050.87397	-3.02	0.68	A

Table 2—Continued

JD (-2450000)	RV ($m\,s^{-1}$)	Error ($m\,s^{-1}$)	Observatory
5051.86595	-2.08	0.53	A
5052.88848	-2.74	0.66	A
5053.88182	-3.97	0.54	A
5054.86448	-2.46	0.56	A
5055.85374	2.20	0.53	A
5058.89140	-1.51	0.59	A
3369.16663	1.69	0.73	K
3425.07667	7.30	0.61	K
3479.96032	0.46	0.58	K
3546.78158	2.94	0.44	K
3547.76796	3.03	0.36	K
3548.80045	-2.27	0.37	K
3549.80104	-0.03	0.37	K
3550.82365	-0.08	0.36	K
3551.80855	-1.31	0.39	K
3576.75813	6.56	0.44	K
3602.72508	5.09	0.49	K
3754.09220	0.80	0.59	K
3776.17013	4.08	0.58	K
3777.08603	1.79	0.56	K

Table 2—Continued

JD (-2450000)	RV ($m\,s^{-1}$)	Error ($m\,s^{-1}$)	Observatory
3806.94545	-1.23	0.58	K
3926.74769	5.03	0.47	K
3927.78252	0.49	0.42	K
3931.82248	-1.03	0.44	K
4131.14294	-7.91	0.65	K
4246.81083	0.59	0.73	K
4247.94552	-2.04	0.72	K
4248.81966	-4.38	1.05	K
4250.80828	0.78	1.09	K
4251.81149	1.78	1.02	K
4255.75898	7.13	0.77	K
4277.73265	-2.06	0.51	K
4278.73377	-5.19	0.86	K
4279.73075	-0.88	0.83	K
4280.74026	-0.24	1.00	K
4285.76472	-6.15	0.63	K
4294.73843	-5.39	0.51	K
4304.73624	4.05	0.60	K
4305.73658	4.59	0.61	K
4306.80060	3.51	0.59	K

Table 2—Continued

JD (-2450000)	RV ($m\,s^{-1}$)	Error ($m\,s^{-1}$)	Observatory
4307.73485	-2.50	0.48	K
4308.73551	2.89	0.56	K
4309.73851	2.20	0.77	K
4310.73545	-1.05	0.84	K
4311.73296	2.89	0.84	K
4312.73423	-0.92	0.53	K
4313.73496	1.04	0.85	K
4314.73608	-2.67	0.87	K
4318.77353	1.92	0.51	K
4455.16774	-0.98	1.19	K
4456.15784	4.78	1.06	K
4465.13890	0.74	1.13	K
4491.10891	7.68	1.08	K
4545.03961	-3.86	1.10	K
4546.03027	4.83	1.21	K
4547.03936	0.14	1.09	K
4600.92698	8.84	1.07	K
4601.87647	7.50	0.97	K
4634.78181	8.36	0.94	K
4666.78904	-4.45	0.30	K

Table 2—Continued

JD (-2450000)	RV ($m\,s^{-1}$)	Error ($m\,s^{-1}$)	Observatory
4667.78945	-1.98	0.29	K
4671.80264	-2.79	0.30	K
4672.78558	-1.72	0.30	K
4673.79754	-2.59	0.29	K
4675.79484	-2.07	0.51	K
4701.73724	2.44	0.36	K
4702.73348	4.02	0.35	K
4703.73110	-1.75	0.46	K
4819.16638	1.75	0.37	K
4820.17627	3.19	0.47	K
4821.14761	0.74	0.85	K
4822.14603	-2.32	0.64	K
4823.16898	0.83	0.38	K
4873.10516	3.59	0.48	K
4903.14262	-3.53	0.45	K
4967.98451	0.49	0.40	K
4968.97445	0.63	0.74	K
5021.83208	4.26	0.32	K
5022.84171	5.41	0.30	K
5023.74658	3.31	0.30	K

Table 2—Continued

JD (-2450000)	RV ($m\,s^{-1}$)	Error ($m\,s^{-1}$)	Observatory
5024.84232	2.22	0.29	K
5049.76443	-2.85	0.29	K
5050.76541	-1.49	0.28	K
5051.75441	-1.87	0.30	K
5052.75467	-0.73	0.33	K
5053.76245	-1.65	0.34	K

Table 3. Circular Orbit Solutions (Epoch JD 2453369.166)

Planet	Period (days)	M (degrees)	e	ω (degrees)	K ($m\,s^{-1}$)	$M \sin i$ ($M_\oplus$)	a (AU)
61 Vir b	4.2149±0.0006	268±13	0	n/a	2.09±0.23	5.1±0.6	0.050201±0.000005
61 Vir c	38.012±0.036	210±16	0	n/a	3.58±0.25	18.2±1.3	0.2175±0.0001
61 Vir d	123.98±0.40	77±33	0	n/a	3.18±0.29	24.0±2.2	0.478±0.001

Table 4. Keplerian Orbital Solutions (Epoch JD 2453369.166)

Planet	Period (days)	M (degrees)	e	ω (degrees)	K ($m\,s^{-1}$)	$M \sin i$ ($M_\oplus$)	a (AU)
61 Vir b	4.2150±0.0006	166±53	0.12±0.11	105±54	2.12±0.23	5.1±0.5	0.050201±0.000005
61 Vir c	38.021±0.034	177±40	0.14±0.06	341±38	3.62±0.23	18.2±1.1	0.2175±0.0001
61 Vir d	123.01±0.55	56±25	0.35±0.09	314±20	3.25±0.39	22.9±2.6	0.476±0.001